ISSN 1063-7761, Journal of Experimental and Theoretical Physics, 2016, Vol. 123, No. 3, pp. 511–519. © Pleiades Publishing, Inc., 2016.
Original Russian Text © V.I. Kuz'min, S.V. Nikolaev, S.G. Ovchinnikov, 2016, published in Zhurnal Eksperimental'noi i Teoreticheskoi Fiziki, 2016, Vol. 150, No. 3, pp. 592–601.

ELECTRONIC PROPERTIES OF SOLID

Effect of Canted Antiferromagnetic Order on the Electronic Structure in the *t–J** Model within the Cluster Perturbation Theory

V. I. Kuz'min[a]*, S. V. Nikolaev[a, b], and S. G. Ovchinnikov[a, b]

[a] *Kirensky Institute of Physics, Siberian Branch, Russian Academy of Sciences, Krasnoyarsk, 660036 Russia*

[b] *Siberian Federal University, Krasnoyarsk, 660041 Russia*

* *e-mail: kuz@iph.krasn.ru*

Received April 4, 2016

Abstract—The electronic structure in the two-dimensional *t–J** model with canted antiferromagnetic order in an external magnetic field has been calculated within the cluster perturbation theory. In zero external field, the evolution of the Fermi surface with *n*-type doping has been obtained in good agreement with experimental data on cuprate superconductors. It has been shown that the inclusion of short-range correlations can result in a nonmonotonic dependence of the spectral weight distribution at the Fermi level on the external magnetic field. In contrast to the case of electron doping, such changes in the case of hole doping can be expected at experimentally achievable fields.

DOI: 10.1134/S1063776116090065

1. INTRODUCTION

Strongly correlated electron systems possess interrelation between the electronic and magnetic (as well as charge) structures, which is most clearly manifested at transitions of the system between states with different spin or charge orders. In view of this circumstance, the relation between Fermi surfaces reconstructed from angle-resolved photoemission spectroscopy (ARPES) data [1–5] and experiments on quantum oscillations [6–14] with high-temperature superconductors is of particular importance. The ARPES data concerning the Fermi surfaces of cuprates are usually in agreement with calculations within strong electron correlation models. The frequencies of quantum oscillations obtained at hole doping $p \approx 0.11$ are an order of magnitude lower than those at $p \approx 0.31$. A similar result was obtained within the strong coupling perturbation theory for the Hubbard model [15]. However, in contrast to ARPES experiments, experiments on quantum oscillations are performed in strong magnetic fields which can exceed 60 T. This means that the electronic structures observed in these two types of experiments can correspond to different regimes. In particular, it was reported that a long-range charge order emerges in a magnetic field in the $La_{2-x}Ba_xCuO_4$ and $YBa_2Cu_3O_y$ compounds at hole doping $p \approx 1/8$ [16]. Quantum oscillation data [17] for $YBa_2Cu_3O_y$ at doping $p \approx 0.11$ for a Fermi surface with an electron pocket in the nodal direction and two hole pockets near it are in agreement with calculations within a phase with a charge density wave [18].

Thus, it is of interest to study changes in the electronic structure of strongly correlated electron systems in the external magnetic field at a fixed doping; such a study is reported in this work. The situation with cuprates at doping $p \gtrsim 0.05$ is very complicated because of the presence of incommensurate magnetic and charge orders [19]. We focus on the cases of hole doping $p \lesssim 0.03$ and electron doping $n \lesssim 0.15$. In these cases, there is a long-range antiferromagnetic order or a short-range order but with a large correlation length [20, 21]. Under these conditions, it can be expected that the external field can affect the electronic structure through a magnetic subsystem, which is an antiferromagnet canted in the external field. It is known that the Néel temperature in the *t–J* model [22, 23] decreases with an increase in doping and vanishes. In particular, it was shown that the transition in the case of hole doping corresponds to values for cuprates [24]. In our approach, the magnetic order is preset and we consider zero temperature. For this reason, we will study below the evolution of the electronic structure with the variation of the magnetic field at fixed levels of *p*- and *n*-type doping at which the long-range magnetic order exists in cuprates.

This work continues work [25], where we studied the evolution of the electronic structure of the *t–J* model at hole doping in the external magnetic field within the mentioned magnetic mechanism. It was shown that a change in the magnetic field by a value of about $0.01J$ (approximately 10 T) does not usually lead to a significant modification of the electronic structure; a noticeable evolution occurs at changes in the

range of approximately $(0.1–1)J$. However, the spectral weight distribution on the Fermi surface can change sharply near a certain field h_c, which depends on the parameters of the model and can be near $0.01J$. Consequently, the Fermi surfaces corresponding to regimes of ARPES and experiments on quantum oscillations can be noticeably different. In this work, as a reason for such a phenomenon, we discuss in detail crossover in multielectron states forming the band structure of quasiparticles. We study the effect of the magnetic order on the electronic structure of *n*- and *p*-type cuprates within the full effective low-energy model for the Hubbard model in the second order of perturbation theory in the parameter t/U, i.e., the *t*–*J* model with three-center interactions [23] (we denote it as *t*–*J**). The effect of three-site terms in the paramagnetic phase is manifested primarily in the high-energy part of the spectrum [26]. However, in the presence of an antiferromagnetic background, the probability of hoppings for the nearest neighbors decreases because such hoppings require spin flip. On the contrary, the nearest correlated three-site hoppings do not perturb the antiferromagnetic environment because they occur within the antiferromagnetic sublattice. Then, a significant effect of the three-site interactions on the electronic structure at low energies is not excluded in the antiferromagnetic case.

The article is organized as follows. The cluster perturbation theory in the *X*-operator representation for the *t*–*J** model, as well as an approximation used to consider the magnetic phase, is briefly described in Section 2. Crossovers in multielectron states, which can be responsible for fast changes in the spectral weight distribution, are discussed in Section 3. Sections 4 and 5 present the results concerning the effect of the external magnetic field on the electronic structure of the *t*–*J** model for the *p*- and *n*-type doping, respectively. In the case of electron doping, we also discuss the doping-induced evolution of the electronic structure in zero field. The main conclusions of this work are presented in the final section.

2. MODEL AND METHOD

Since the effect of the magnetic field on the electronic structure is taken into account in this work exclusively through the magnetic order, we include the Zeeman term and neglect the orbital contribution. The corresponding Hamiltonian of the *t*–*J** model in the external magnetic field has the form

$$H_{t-J^*} = H_{t-J} + H_3 + H_Z. \quad (1)$$

Here,

$$H_{t-J} = -\sum_{i,j,\sigma}(t_{i,j}c^{\dagger}_{i,\sigma}c_{j,\sigma} + \text{H.c.}) + \frac{J}{2}\sum_{\langle i,j\rangle}\left(\mathbf{S}_i\cdot\mathbf{S}_j - \frac{n_i n_j}{4}\right), \quad (2)$$

$$H_3 = -\frac{J}{4}\sum_{i,\sigma}\sum_{\delta\neq\delta'}(c^{\dagger}_{i+\delta,\sigma}n_{i,\bar{\sigma}}c_{i+\delta',\sigma} - c^{\dagger}_{i+\delta,\sigma}c^{\dagger}_{i,\bar{\sigma}}c_{i,\sigma}c_{i+\delta',\bar{\sigma}}), \quad (3)$$

where $c^{\dagger}_{i,\sigma}$ and $c_{i,\sigma}$ are the quasi-fermion creation and annihilation operators for a particle with the spin σ at the *i*th site, respectively; $\bar{\sigma} = -\sigma$; $t_{i,j}$ is the hopping integral; J is the indirect exchange integral related to the Coulomb repulsion parameter in the Hubbard model as $J = 4t^2/U$; and $\mathbf{S}_i$ is the spin operator; and

$$H_Z = -h\sum_i \mathrm{S}^z_i,$$

where h is the energy of the magnetic field.

To calculate the spectral weight in the *t*–*J** model, we used the cluster perturbation theory based on the exact diagonalization method [27, 28]. In the cluster perturbation theory, short-range interactions are taken into account within a finite cluster, whereas long-range interactions are taken into account by perturbation theory. Within the cluster perturbation theory, the initial lattice is covered by translations of a cluster with chosen size and shape. Then, the exact diagonalization of the cluster is performed and the cluster Green's function is calculated. Further, the intercluster interactions are taken into account by perturbation theory in the Hubbard-I approximation. After that, Fourier transformation to the paramagnetic Brillouin zone is performed with the use of the long-wavelength approximation to obtain the Green's function of the lattice $G(\mathbf{k}, \omega)$ [28]. We use the version of the cluster perturbation theory based on the *X*-operator technique, i.e., the so-called norm-conserving cluster perturbation theory [29, 30]. In this approach, the full Hilbert space of the cluster is taken into account, which makes it possible to control the total spectral weight of quasiparticles in all stages of calculation. In order to appropriately take into account the presence of canted antiferromagnetism, we specify the corresponding symmetry of cluster states by means of the introduction of a mean field as was done in [31, 32] for the Heisenberg model.

We cover the lattice by translations of a 2×2 square cluster in the translation directions of the initial square lattice. The cluster of four sites allows taking into account the main qualitative features of the spectral weight distribution. It was shown that a five-site cluster in the paramagnetic case makes it possible to achieve almost quantitative agreement for the spectral weight distribution in the Hubbard model with the quantum Monte Carlo results [33]. It is reasonable to expect that the Hubbard-I approximation is more efficient in the antiferromagnetic case than in the paramagnetic phase because of a larger contribution of long-range effects.

For an antiferromagnet in the external magnetic field directed along the z axis perpendicular to the plane, there are two magnetization components–the

in-plane antiferromagnetic component and the constant component along the field. It is convenient to orient the x axis along the antiferromagnetic component ($\langle S_i^y \rangle = 0$). We first regroup terms in Hamiltonian (1):

$$H = \sum_f h_c(f) + \sum_{f,g} h_{cc}^1(f,g) + \sum_{f,g} h_{cc}^2(f,g) + \sum_{f,g,h} h_{ccc}(f,g,h), \quad (4)$$

where f and g are the cluster indices, h_{cc}^2 is the Heisenberg part of the intercluster interaction, h_{ccc} includes three-center hoppings connecting three clusters, and h_{cc}^1 includes all remaining terms of the Hamiltonian. To introduce mean fields acting on the cluster, we identically transform the term h_{cc}^2 as

$$\frac{J}{2}\sum_{\substack{f\neq g\\ \langle ij\rangle}} (S_{f,i}^x S_{g,j}^x + S_{f,i}^y S_{g,j}^y + S_{f,i}^z S_{g,j}^z) \equiv \sum_{\substack{f\neq g\\ \langle ij\rangle}} \Delta h_{cc}^2(f,g) + \sum_f (\Delta_x(f) + \Delta_z(f)), \quad (5)$$

where

$$\sum_{\substack{f\neq g\\ \langle ij\rangle}} \Delta h_{cc}^2(f,g) = \frac{J}{2}[(S_{f,i}^x - \langle S_{f,i}^x\rangle)(S_{g,j}^x - \langle S_{g,j}^z\rangle) + S_{f,i}^y S_{g,j}^y + (S_{f,i}^z - \langle S_{f,i}^z\rangle)(S_{g,j}^z - \langle S_{g,j}^z\rangle)], \quad (6)$$

$$\Delta_x(f) = \frac{J}{2}\left(4\sigma_x^2 + 2\sigma_x \sum_{i=1}^4 (-1)^i S_{f,i}^x\right),$$
$$\Delta_z(f) = \frac{J}{2}\left(-4\sigma_z^2 + 2\sigma_z \sum_{i=1}^4 S_{f,i}^z\right). \quad (7)$$

In Eqs. (5)–(7) and below, the subscripts i and j specify sites within the clusters and $\sigma_x = |\langle S_i^x\rangle|$ and $\sigma_z = \langle S_i^z\rangle$ in Eqs. (7) are the order parameters. Then, we redefine the terms in Eq. (4) in order to include the mean field in the local part h_c:

$$h_c(f) \to h_c(f;\sigma_x,\sigma_z) = h_c(f) + \Delta_x(f) + \Delta_z(f),$$
$$h_{cc}^2(f,g) \to \Delta h_{cc}^2(f,g;\sigma_x,\sigma_z). \quad (8)$$

Similar to [31, 32], we determine the parameters σ_x and σ_z from the system

$$\sigma_x = \langle S_1^x\rangle_0, \quad \sigma_z = \langle S_1^z\rangle_0, \quad (9)$$

where the space symmetry of the cluster is used. The zeroth average in Eqs. (9) implies averaging over the Hamiltonian h_c.

Below, we follow the standard scheme of the norm-conserving cluster perturbation theory [29, 30]. We define the X-operators $X^\alpha \equiv X^{pq} = |p\rangle\langle q|$ on the complete basis of cluster states. Thus, the electron is represented as a linear combination of Hubbard fermions each describing a local excitation from the initial state $|q\rangle$ with n electrons to the final state $|p\rangle$ with $n-1$ electrons. This representation allows a significant reduction of the number of eigenstates taken into account in the local Hilbert space. To control this procedure, we use the sum rule presenting the total spectral weight of the electron. The quantity specifying the spectral sum rule is defined as

$$W_\sigma = \langle [c_{\mathbf{k},\sigma}, c_{\mathbf{k},\sigma}^\dagger]_+\rangle = n^0 + n^\sigma = \frac{1 \pm 2\sigma_z + n^0}{2}, \quad (10)$$

where the sign $\pm$ corresponds to the spin projection along/against the field, n^0 is the concentration of empty sites, and n^σ is the concentration of particles with the spin σ. We introduce the quantity $f_{i,\sigma}$ in order to conserve only those Hubbard fermions that have a significant spectral weight and, thereby, to significantly reduce the computation time:

$$f_{i,\sigma} = \sum_\alpha |\gamma_{i,\sigma}(\alpha)|^2 F(\alpha), \quad (11)$$

where summation involves only the transitions that are retained, $\gamma_{i,\sigma}$ are the matrix elements of the operators $c_{i\sigma}$ in the X-operator representation and

$$F(\alpha) \equiv F(p,q) = \langle X^{pp}\rangle + \langle X^{qq}\rangle \quad (12)$$

is the filling factor. When all transitions are taken into account in Eq. (11), $f_{i,\sigma} = W_\sigma$. In this work, $f_{i,\sigma} \geq W_\sigma - 0.001$.

As usual in the cluster perturbation theory, the intercluster interactions are considered in the Hubbard-I approximation. The Green's function

$$D_{\alpha\beta}(\tilde{\mathbf{k}},\omega) = \langle\langle X_{\tilde{\mathbf{k}}}^\alpha | X_{\tilde{\mathbf{k}}}^{-\beta}\rangle\rangle_\omega,$$

which is defined in the reduced Brillouin zone, is calculated from the matrix equation

$$D^{-1}(\tilde{\mathbf{k}},\omega) = [D^0(\omega)]^{-1} - T(\tilde{\mathbf{k}}) - T^*(\tilde{\mathbf{k}}) - V, \quad (13)$$

where $D^0(\omega)$ is the cluster Green's function, the matrices $T(\tilde{\mathbf{k}})$ and $T^*(\tilde{\mathbf{k}})$ are due to the disconnection of Green's functions appearing at the calculation of commutators with the kinetic term and term responsible for three-site hoppings between two clusters, and the matrix V appears similarly from the exchange contribution and three-site hoppings connecting three clusters. The electron Green's function in the para-

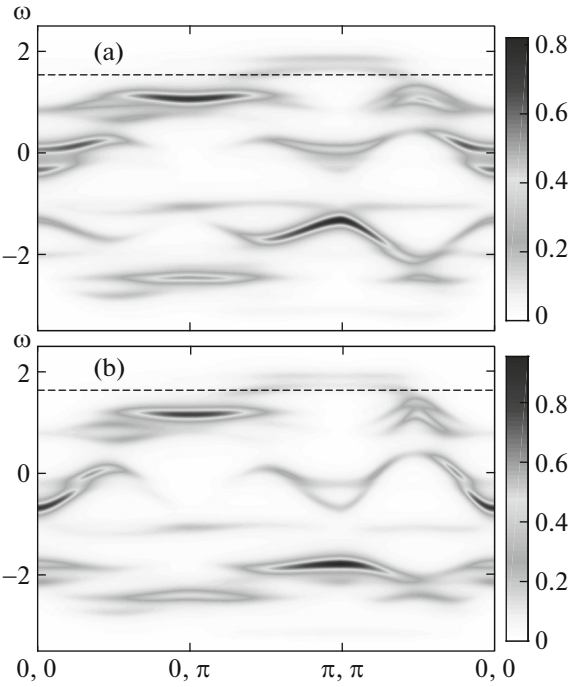

Fig. 1. Electron spectral function along the symmetric directions of the first Brillouin zone in the (a) t–J and (b) t–J^* models at $t' = t'' = 0$, $J = 0.25t$, and order parameters $\sigma_x \approx 0.41$ and $\sigma_z = 0$. Here and in similar plots below, the dashed line denotes the position of the Fermi level and we use the Lorentzian broadening with the half-width $\delta = 0.1t$.

magnetic Brillouin zone is reconstructed by the formula [28]

$$G_\sigma(\mathbf{k},\omega) = \frac{1}{N_c}\sum_{\alpha,\beta}\sum_{i,j=1}^{N_c}\gamma_{\sigma i}(\alpha)\gamma^*_{\sigma j}(\beta) \times e^{-i\mathbf{k}(\mathbf{r}_i-\mathbf{r}_j)}D_{\alpha\beta}(\mathbf{k},\omega), \quad (14)$$

where N_c is the number of sites in the cluster.

Figure 1 shows the spectral weights obtained disregarding three-center correlated hoppings in comparison with that obtained taking into account these hoppings in zero magnetic field. Here and below, the energy of quasiparticles ω is measured in units of $|t| \sim 0.25$–0.4 eV [3, 5], where t is the hopping integral between the nearest neighbors. We also take into account hoppings between the second t' and third t'' neighbors. The delta function at the poles of the Green's function is approximated by a Lorentzian with a finite half-width δ for the representation of spectral weight distributions in the form similar to that of ARPES data. The electronic structure in the lower (or upper) Hubbard band can be generally represented as a structure split into two bands in agreement with quantum Monte Carlo results [34]. The low-energy part of the electronic structure shown in Fig. 1, which was calculated within both the t–J and t–J^* models, is characteristic of dispersion in the presence of spin fluctuations [35–41]. As in the paramagnetic phases, the main differences between the results obtained with and without the inclusion of the three-center interactions are manifested at the high-energy scale, whereas no significant changes are observed in the low-energy structure in the presence of antiferromagnetism too. However, differences in the weight distribution can significantly affect the position of the Fermi level and, consequently, the form of the Fermi surface. The described difference is revealed in this work, but the main conclusions of work [25] hold, as will be shown below.

3. CROSSOVERS IN MULTIELECTRON STATES

The electronic structure in our calculations depends on the order parameters, which are determined self-consistently for an individual cluster and affect cluster wavefunctions specifying in turn the electronic structure. We consider the expansion of the wavefunction in the form

$$|n\rangle = \sum_{s,m,q}\tilde{c}^q_{sm}|s,m\rangle_q = \sum_{s,m}c_{sm}|s,m\rangle, \quad (15)$$

where $|n\rangle$ is an eigenfunction of the Hamiltonian of the cluster; s and m are the total spin of the cluster and its projection on the z axis, respectively; $|s, m\rangle_q$ are the eigenfunctions of the cluster operators $\mathbf{S}^2$ and S^z (a cluster operator is given by the expression $\mathbf{S} = \sum_i \mathbf{S}_i$, where summation is performed over sites in the cluster); and the index q is due to degeneracy in s and m owing to the geometry of the cluster.

The dependence of the electronic structure of the cluster in the subspace with three particles has specific a feature—crossover of lower levels at the magnetic field $h \approx 1J$ in the case of the inclusion of only the nearest hoppings (see Fig. 2). As is seen in Fig. 3, a transition occurs from a low-spin state with the dominant component $|0.5, 0.5\rangle$ to a high-spin state with the dominant component $|1.5, 1.5\rangle$. The ground state in this sector is doubly degenerate at fields $h < h_c$ and is nondegenerate at $h > h_c$. This effect can be responsible for a nonmonotonic behavior of the electronic structure of quasiparticles. In our case, this effect is due to the inclusion of short-range correlations in the presence of the mean field acting on the cluster. The nearest and next-nearest neighbors can be taken into account in the 2 × 2 cluster. For this reason, the parameters t' and J affect the h_c value: with an increase in the amplitudes of the second hoppings and at a fixed exchange integral, the h_c value decreases in the case of the p type and increases for the n type. With the model parameters characteristic of p-type cuprates, we obtain the field $h_c \sim 0.01J \sim 10$ T and, correspondingly, can expect significant changes in the Fermi surface in this region of fields. The crossover field

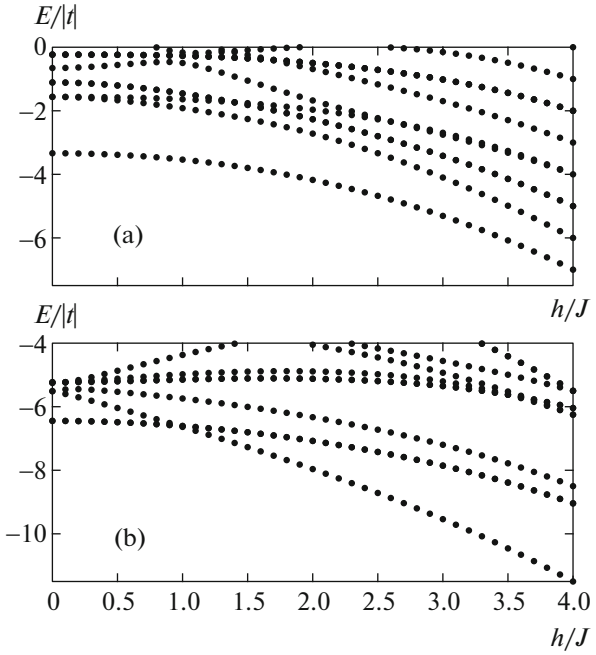

Fig. 2. Magnetic-field dependence of the low-energy part of the electronic structure of the cluster in the sectors of the Hilbert space with (a) four and (b) three particles at $J = 0.333t$, $t' = t'' = 0$, and $p = 0$.

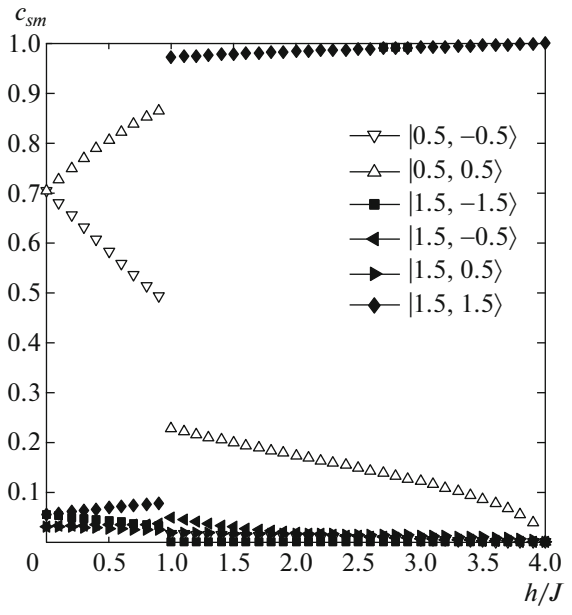

Fig. 3. Coefficients c_{sm} defined in Eq. (15) for the wavefunction of the ground state in the subspace with three electrons per cluster at $J = 0.333t$, $t' = t'' = 0$, and $p = 0$.

obtained with the parameters characteristic of the *n* type is much higher ($h_c \sim 1J \sim 1000$ T) than experimentally achievable fields.

4. EFFECT OF THE MAGNETIC FIELD ON THE ELECTRONIC STRUCTURE, *p* TYPE

We consider the evolution of the electronic structure in our approach at *p*-type doping. For definiteness, we use in this section the hopping integral for the second neighbors $t' = -0.15t$ typical of $La_{2-x}Sr_xCuO_4$ [3, 42]. If the exchange integral is $J = 0.25t$, the crossover field is $h_c \approx 0.02J$, which is of interest for achievable experiments. In this section, hole doping is $p = 0.02$.

For completeness, we first mention the main characteristics of evolution of the spectral weight distribution depending on the rearrangement of the magnetic structure in the external field according to the calculation within the t–J* model (see Fig. 4). They qualitatively coincide with the characteristics obtained disregarding three-site hoppings [25]. At a field of $4J$, when the ferromagnetic saturation is achieved [43], the dispersion law with a band width of $8t$ and a uniform spectral weight distribution over the entire band is observed for up spin; this dispersion law is inherent in the spatially uniform phase. For down spin, there is a narrow band with a small spectral weight at the Fermi level (see Fig. 4). At a lower field, e.g., $h = 3J$, the electron dispersion law is modified owing to the mixing of different spin states. In this case, the dispersion law for down spin is similar to that for the shadow subband of the two-sublattice system. The spectral weight distribution and dispersion law at $h = 0.5J$ and zero field are qualitatively similar.

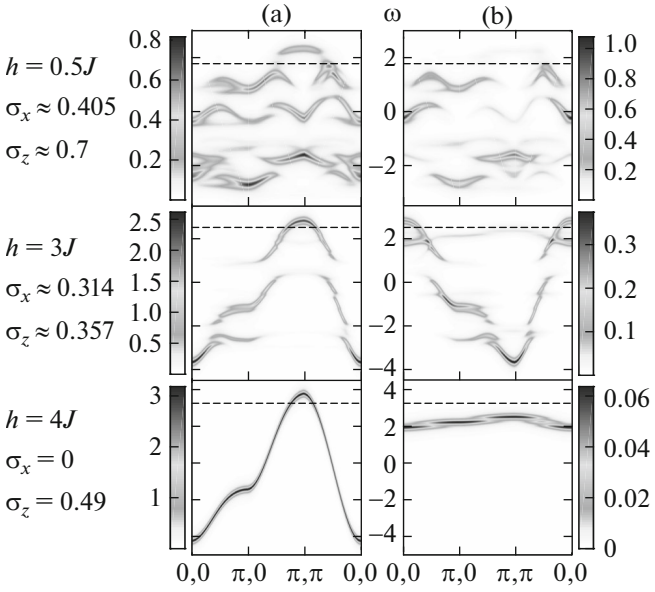

Fig. 4. Electron spectral function along the symmetric directions of the first Brillouin zone at various magnetic fields for (a) up and (b) down spins at the parameters $t' = -0.15t$, $t'' = 0.1t$, $J = 0.25t$, and $p = 0.02$.

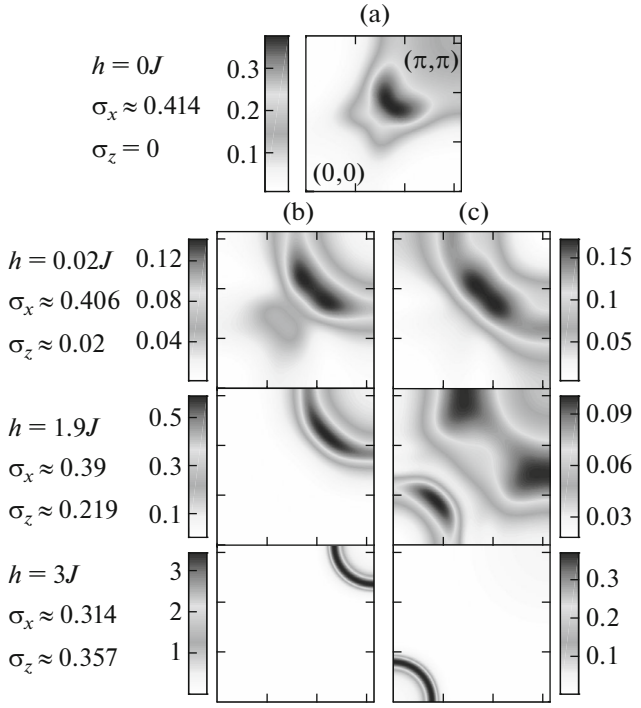

Fig. 5. Spectral weight distribution at the Fermi level in the first quadrant of the Brillouin zone (a) in zero external field for one spin projection and (b, c) in various fields for (a) up and (b) down spins at the parameters $t' = -0.15t$, $t'' = 0.1t$, and $J = 0.25t$. Here and in similar plots below, we use the Lorentzian broadening with the half-width $\delta = 0.04t$ and the spectral weight is averaged over the energy window $[-1.5\delta, 1.5\delta]$.

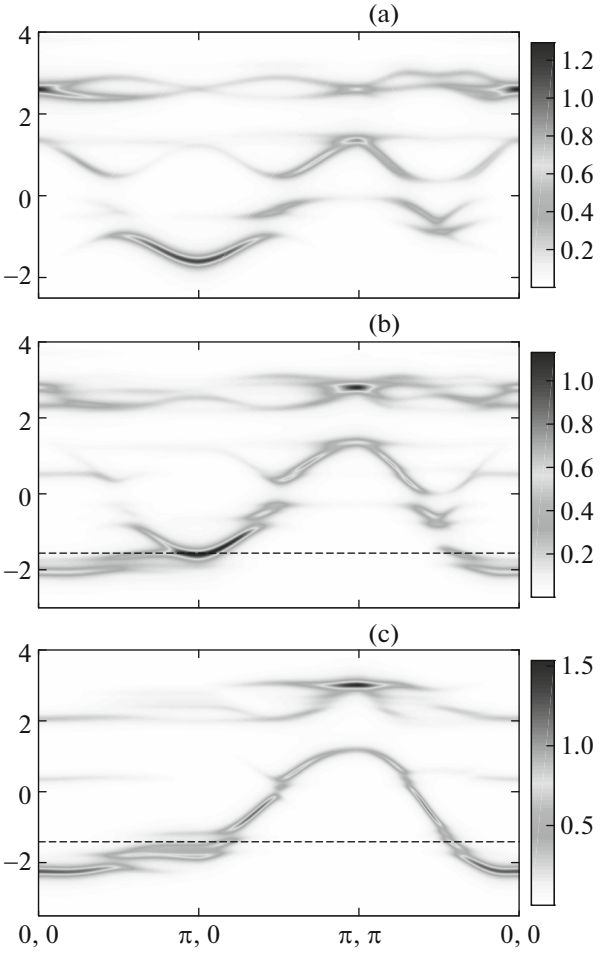

Fig. 6. Electron spectral function along the symmetric directions of the first Brillouin zone in zero external field at the antiferromagnetic order parameter (a) $\sigma_x \approx 0.438$ at zero electron doping, (b) $\sigma_x \approx 0.331$ at $n = 0.1$, and (c) disregarding the mean field ($\sigma_x = 0$) at $n = 0.2$.

The modification of the spectral weight at the Fermi level in the magnetic field is shown in Fig. 5. The distribution in zero field has a pronounced maximum in the nodal direction ($(0, \pi) \to (\pi, \pi)$). Such a distribution can be conditionally characterized as a "pocket" because it is similar to the spectral weight distribution for a Fermi pocket calculated with a significant broadening of spectral lines [30]. As in the case of ARPES, the resulting Fermi surfaces are due to averaging over an energy range near the Fermi level rather than simply follow from the single isoenergetic surface at the Fermi level (see the caption of Fig. 5). On the other hand, in the field $h \sim 3J$, there are pockets around the point (π, π) for up spin and around the point (0, 0) for down spin. The spectral weight is uniformly distributed along the edges of pockets and differs by an order of magnitude for two spin projections. An increase in the magnetic field to the saturation value does not qualitatively change the Fermi surface for up spin, but the weight on the Fermi surface for down spin almost vanishes (see Fig. 4). In the interval from $h = 0$ to $h \sim 3J$, the spectral weight distribution is gradually smoothed. The distributions for the dominant spin component for the presented values $h = 0.02J$ and $h = 1.9J$ are insignificantly different. For down spin, no significant changes are observed in the interval of fields from $h = 0.02J$ to $h \sim 0.2J$. Nevertheless, owing to the crossover of cluster states, which was discussed in Section 3, an increase in the field from $h = 0$ to $h = 0.02J$ is accompanied by a sharp change in the spectral weight distribution along the antinodal direction ($(0, \pi) \to (\pi, \pi)$) for both components, which, for the projection along the field, can be characterized as a transition from a pocket distribution to an arc distribution. We assume that, if similar nonmonotonic changes occur in underdoped hole-type cuprates, they can be detected in transport measurements.

5. EFFECT OF DOPING AND THE MAGNETIC FIELD ON THE ELECTRONIC STRUCTURE, *n* TYPE

Since *n*-type cuprates have an antiferromagnetic order in a wide range of doping up to the optimal level

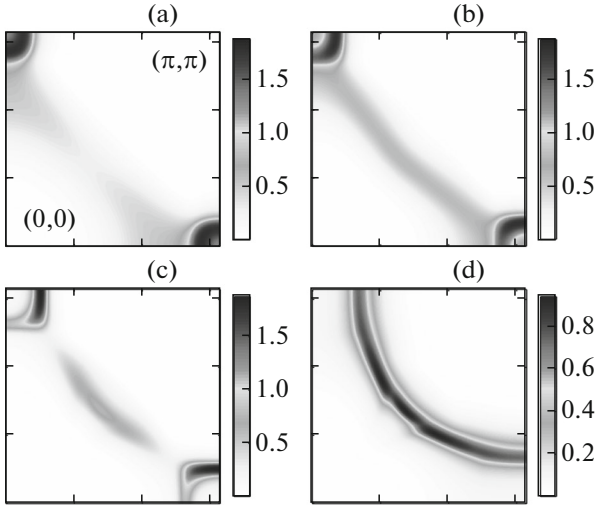

Fig. 7. Spectral weight distribution at the Fermi level in the first quadrant of the Brillouin zone in zero external field. Doping level and the corresponding antiferromagnetic parameters assume the following values: (a) $n = 0.05$ and $\sigma_x = 0.384$, (b) $n = 0.1$ and $\sigma_x = 0.331$, (c) $n = 0.15$ and $\sigma_x = 0.28$, and (d) $n = 0.2$ disregarding the mean field ($\sigma_x = 0$).

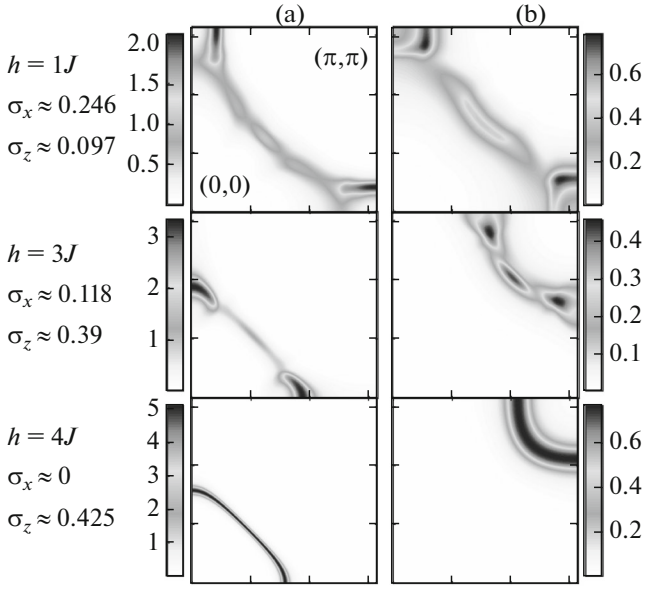

Fig. 8. Spectral weight distribution at the Fermi level in the first quadrant of the Brillouin zone in various external fields h for (a) up and (b) down spins at the doping $n = 0.15$.

$n \sim 0.15$, we consider the doping-induced evolution of the electronic structure in zero magnetic field. In this section, we use the hopping parameters $t' = -0.2t$ and $t'' = 0.1t$ typical of the $Nd_{2-x}Ce_xCuO_4$ compound [5] and a value of $0.333J \approx 0.1$ eV is chosen for the exchange integral.

The main features of the spectral weight distribution with and without doping are illustrated in Fig. 6. The bottom of the band at $n = 0$ is near the point $(\pi, 0)$; it has the largest spectral weight and plays the main role in the formation of the Fermi surface at low doping. The dispersion segment near the point (π, π) is less intense. Doping results in the appearance of a flat quasiparticle band under the Fermi level. The presented weight distribution in the lower subband of the upper Hubbard band ($\omega \sim -2$ to $+2$) is qualitatively similar to weight distributions obtained within the dynamical mean field theory for multiband models of n-type cuprates [44, 45]. The region near the energy $\omega \sim 0$ and along the directions $(\pi, 0) \to (\pi, \pi)$ and $(\pi, \pi) \to (\pi/2, \pi/2)$, where the splitting of the dispersion law into individual branches is pronounced, corresponds to the regions with the pronounced damping of quasiparticle dispersion in dynamical-mean-field-theory calculations [44]. According to the calculation for doping $n = 0.2$ (Fig. 6c), when the long-range order is absent, the concave fragment of dispersion near the point $(\pi, 0)$ (see Figs. 6a, 6b) is absent and the gap near the point $(\pi/2, \pi/2)$ is almost closed.

The evolution of the Fermi surface with doping in zero external magnetic field is shown in Fig. 7. At doping $n = 0.05$, the main contribution to the spectral weight comes from electron pockets near the points $(\pi, 0)$ and $(0, \pi)$. A further increase in doping up to the optimal value (see Figs. 7a–7c) results in an increase in the spectral weight from holes near $(\pi/2, \pi/2)$. At $n = 0.15$, the spectral weight has a dip near the so-called "hot points" typical of optimally doped electron-type cuprates [5]. The Fermi surface obtained are in good agreement with the ARPES data [5, 46]. In order to reproduce the evolution of the Fermi surface qualitatively consistent with the ARPES data, it was necessary to take into account both the long-range magnetic order and short-range antiferromagnetic fluctuations. Figure 7d also shows the Fermi surface calculated with $n = 0.2$ in zero mean field for the case where the long-range magnetic order should be destroyed. In this case, the hole surface is large, whereas both electron and hole carriers contribute to the spectral weight at the optimal doping and electron-like carriers make a larger contribution on the Fermi surface at $n = 0.15$. Our calculations imply that a change in the sign of the Hall constant in the normal state of various n-type cuprates with an increase in doping [47–49] is due to a change in the magnetic order.

We now consider the magnetic-field-induced evolution of the Fermi surface for n-type cuprates. As was mentioned above, in the case of electron doping, the field h_c is about J; for the given set of parameters, $h_c \approx 1.88J$. In this case, a jump in the spectral weight hardly changes the Fermi surface. Figure 8 illustrates the magnetic-field-induced evolution of the Fermi surface. Fields $h \sim 0.1J \sim 100$ T provide insignificant effect. The surface at scale $h \sim J$ is gradually transformed to pockets near the points $(0, 0)$ and (π, π) for

up and down spins, respectively. This property is manifested in the entire doping range under consideration.

6. CONCLUSIONS

The effect of the magnetic field on the electronic structure through the interrelation of the magnetic and electronic subsystems, which is inherent in strongly correlated systems, has been studied within the t–J^* model. Both hole and electron doping have been considered. Crossovers in cluster states have been analyzed and it has been shown that they can be responsible for a nonmonotonic dependence of the spectral weight distribution on the Fermi surface on the external magnetic field. In addition, the electronic structure with doping has been studied for the n type. The main conclusions of this work are as follows.

At low hole doping, there are the parameters of the model at which we have obtained a crossover in multielectron states and the corresponding sharp change in the spectral weight distribution at the Fermi level in the magnetic field h_c corresponding to the experimentally achievable value. We have considered the case with $h_c \approx 0.02J \sim 20$ T. In the case of electron doping, the field h_c is about $J \sim 1000$ T and, as a result, significant changes in the Fermi surface in realistic fields are not observed. In view of this circumstance, we emphasize that, in contrast to the case of hole doping, for n-type doping, the Fermi surfaces reconstructed from experiments on quantum oscillations [13] in the range $n = 0.15$–0.17 qualitatively coincide with the ARPES Fermi surface [5, 46]. The inclusion of the long-range antiferromagnetic order, together with short-range correlations, makes it possible to reproduce the evolution of the Fermi surface of n-type cuprates, which is in agreement with the ARPES and quantum oscillation data [13]. The comparison of the calculations with and without the inclusion of the long-range antiferromagnetic order at zero external magnetic field indicates that the sign of the Hall constant changes at the transition from the optimally doped state to overdoped one [47–49] because of the destruction of antiferromagnetism. Change in the sign of the Hall constant at the transition through a quantum critical point should be revealed in the calculation with a spin-density wave (SDW) disregarding short-range correlations [50]. This result was not obvious a priori in our approach because the resulting Fermi surfaces in the magnetic phase do not directly follow from the potential of the antiferromagnetic superlattice, as in the SDW approach; they are rather obtained from the properties of cluster (multielectron) states. The latter circumstance makes it possible to obtain an asymmetric spectral weight distribution with respect to the edge of the antiferromagnetic Brillouin zone in agreement with the ARPES data.

ACKNOWLEDGMENTS

We are grateful to V.V. Val'kov for stimulating discussions. This work was supported by the Russian Science Foundation (project no. 14-12-00061).

REFERENCES

1. A. Damacelli, Z. Hussein, and Z. X. Shen, Rev. Mod. Phys. **75**, 473 (2003).
2. M. Platé, J. D. F. Mottershead, I. S. Elfimov, et al., Phys. Rev. Lett. **95**, 077001 (2005).
3. T. Yoshida, X. J. Zhou, K. Tanaka, et al., Phys. Rev. B **74**, 224510 (2006).
4. T. Yoshida, M. Hashimoto, S. Ideta, et al., Phys. Rev. Lett. **103**, 037004 (2009).
5. M. Ikeda, T. Yoshida, A. Fujimori, et al., Phys. Rev. B **80**, 014510 (2009).
6. N. Doiron-Leyraud, C. Proust, D. LeBoeuf, et al., Nature **447**, 565 (2007).
7. D. LeBoeuf, N. Doiron-Leyraud, J. Levallois, et al., Nature **450**, 533 (2007).
8. C. Jaudet, D. Vignolles, A. Audouard, et al., Phys. Rev. Lett. **100**, 187005 (2008).
9. S. E. Sebastian, N. Harrison, E. Palm, et al., Nature **454**, 200 (2008).
10. B. Vignolle, A. Carrington, R. A. Cooper, et al., Nature **455**, 952 (2008).
11. C. Jaudet, D. Vignolles, A. Audouard, et al., Phys. Rev. B 82, 140501 (R) (2010).
12. P. M. C. Rourke, A. F. Bangura, T. M. Benseman, et al., New J. Phys. **12**, 105009 (2010).
13. T. Helm, M. V. Kartsovnik, M. Bartkowiak, et al., Phys. Rev. Lett. **103**, 157002 (2009).
14. N. Barišić, S. Badoux, M. K. Chan, et al., Nat. Phys. **9**, 761 (2013).
15. A. Sherman, arXiv:cond-mat/1503.04934.
16. T. Wu, H. Mayaffre, S. Krämer et al., Nature **477**, 191 (2011).
17. N. Doiron-Leyraud, S. Badoux, S. René de Cotret, et al., Nature Comm. **6**, 6034 (2015).
18. A. Allais, D. Chowdhury, and S. Sachdev, Nature Comm. **5**, 5771 (2014).
19. J. M. Tranquada, B. J. Sternlieb, J. D. Axe, et al., Nature **375**, 561 (1995).
20. B. Keimer, N. Belk, R. J. Birgeneau, et al., Phys. Rev. B **46**, 14034 (1992).
21. E. M. Motoyama, G. Yu, I. M. Vishik, et al., Nature Lett. **445**, 187 (2007).
22. L. N. Bulaevskii, E. L. Nagaev, and D. L. Khomskii, Sov. Phys. JETP **27**, 836 (1968).
23. K. A. Chao, J. Spalek, and A. M. Oles, J. Phys. C: Condens. Matter **10**, L271 (1977).
24. J. L. Richard and V. Yu. Yushankhai, Phys. Rev. B **50**, 12927 (1994).
25. V. I. Kuz'min, S. V. Nikolaev, and S. G. Ovchinnikov, JETP Lett. **103**, 125 (2016).
26. V. I. Kuz'min, S. V. Nikolaev, and S. G. Ovchinnikov, Phys. Rev. B **90**, 245104 (2014).

27. D. Senechal, D. Perez, and M. Pioro-Ladriere, Phys. Rev. Lett. **84**, 522 (2000).
28. D. Senechal, D. Perez, and D. Plouffe, Phys. Rev. B **66**, 075129 (2002).
29. S. V. Nikolaev and S. G. Ovchinnikov, J. Exp. Theor. Phys. **111**, 635 (2010).
30. S. V. Nikolaev and S. G. Ovchinnikov, J. Exp. Theor. Phys. **114**, 118 (2012).
31. V. V. Val'kov, V. A. Mitskan, and G. A. Petrakovskii, J. Exp. Theor. Phys. **102**, 234 (2006).
32. V. V. Val'kov and V. A. Mitskan, J. Exp. Theor. Phys. **105**, 90 (2007).
33. A. S. Krinitsyn, S. V. Nikolaev, and S. G. Ovchinnikov, J. Supercond. Nov. Magn. **27**, 955 (2014).
34. C. Gröber, R. Eder, and W. Hanke, Phys. Rev. B **62**, 4336 (2000).
35. S. G. Ovchinnikov, Phys. Usp. **40**, 966 (1997).
36. A. F. Barabanov, A. A. Kovalev, O. V. Urazaev, A. M. Belemuk, and R. Hayn, J. Exp. Theor. Phys. **92**, 677 (2001).
37. V. V. Val'kov and D. M. Dzebisashvili, J. Exp. Theor. Phys. **100**, 608 (2005).
38. M. Aichhorn, E. Arrigoni, M. Potthoff, and W. Hanke, Phys. Rev. B **74**, 024508 (2006).
39. N. M. Plakida and V. S. Oudovenko, J. Exp. Theor. Phys. **104**, 230 (2007).
40. A. Avella and F. Mancini, Phys. Rev. B **75**, 134518 (2007).
41. A. Avella, Adv. Cond. Mat. Phys. **2014**, 515698 (2014).
42. E. Pavarini, I. Dasgupta, T. Saha-Dasgupta, et al., Phys. Rev. Lett. **46**, 047003 (2001).
43. A. Lüscher and A. M. Läuchli, Phys. Rev. B **79**, 195102 (2009).
44. C. Weber, K. Haule, and G. Kotliar, Phys. Rev. B **82**, 125107 (2010).
45. E. Z. Kuchinskii, I. A. Nekrasov, and N. S. Pavlov, J. Exp. Theor. Phys. **117**, 327 (2013).
46. N. P. Armitage, F. Ronning, D. H. Lu, et al., Phys. Rev. Lett. **88**, 257001 (2002).
47. T. B. Charikova, N. G. Shelushinina, G. I. Harus, et al., Physica C **483**, 113 (2012).
48. Y. Dagan and R. L. Greene, Phys. Rev. B. **76**, 024506 (2007).
49. K. Jin, B. Y. Zhu, B. X. Wu, et al., Phys. Rev. B **78**, 174521 (2008).
50. J. Lin and A. J. Millis, Phys. Rev. B **72**, 214506 (2005).

Translated by R. Tyapaev